# Lattice-Boltzmann-based two-phase thermal model for simulating phase change

M. R. Kamali,* J. J. J. Gillissen, and H. E. A. van den Akker
*Transport Phenomena Group, Department of Chemical Engineering, Delft University of Technology, Delft, Netherlands*

Sankaran Sundaresan
*Chemical and Biological Engineering Department, Princeton University, Princeton, New Jersey 08540, USA*
(Received 2 April 2013; published 13 September 2013)

A lattice Boltzmann (LB) method is presented for solving the energy conservation equation in two phases when the phase change effects are included in the model. This approach employs multiple distribution functions, one for a pseudotemperature scalar variable and the rest for the various species. A nonideal equation of state (EOS) is introduced by using a pseudopotential LB model. The evolution equation for the pseudotemperature variable is constructed in such a manner that in the continuum limit one recovers the well known macroscopic energy conservation equation for the mixtures. Heats of reaction, the enthalpy change associated with the phase change, and the diffusive transport of enthalpy are all taken into account; but the dependence of enthalpy on pressure, which is usually a small effect in most nonisothermal flows encountered in chemical reaction systems, is ignored. The energy equation is coupled to the LB equations for species transport and pseudopotential interaction forces through the EOS by using the filtered local pseudotemperature field. The proposed scheme is validated against simple test problems for which analytical solutions can readily be obtained.

DOI: 10.1103/PhysRevE.88.033302 PACS number(s): 47.11.−j, 02.70.−c, 05.70.Fh, 05.70.Ce

## I. INTRODUCTION

Coupling between thermodynamics and mass, momentum and energy transport, produces a variety of complex problems in fluid dynamics. An example of this is the phase change process due to thermal effects. Simulation of flow with a phase change is challenging as a result of the evolving nature of the fluid-fluid interface. Various numerical schemes, such as the volume of fluid method [1], interface tracking [2,3], the level set method [4], etc., could be used for handling the evolving interface and for the coupling of hydrodynamics, the species and energy transport, with thermodynamics.

The lattice Boltzmann (LB) method offers some advantages in simulating multicomponent multiphase flows by doing away with interface tracking [5–11], but the interface does become diffuse. It also provides a convenient framework to incorporate thermodynamic effects, which naturally generate the phase separation. Multiphase LB methods have been used widely in isothermal flow simulations [12–20]; in contrast, their application to nonisothermal flow simulations has been limited.

A number of authors have investigated rigorous LB methods where the energy balance is recovered as the higher-order velocity moments of the discrete species distribution functions (mass and momentum are conserved by considering the first- and second-order velocity moments) [21–24]. But progress in these methods has been limited especially for thermal two-phase flows due to the high computational demands and numerical instabilities. To the best of our knowledge the application of such approaches to nonisothermal reacting flows has not received much attention.

Hybrid schemes where the flow is simulated using the LB method and the energy balance is solved via conventional computational fluid dynamics (CFD) schemes, such as the finite difference method, have been employed in many studies [25–29]. As a more popular approach, several researchers have explored solutions of the thermal energy balance via a LB method by introducing an extra distribution function, over and above those required to solve the mass and momentum balances, this extra distribution function is evolved in time and space in such a way as to (nearly) recover the desired macroscopic energy balance equation [30–34].

In this article we construct the LB evolution equation for a pseudotemperature variable in such a manner that the macroscopic energy conservation equation for mixtures is recovered in the continuum limit. The mass and momentum transport equations as well as the nonideal equation of state (EOS) are handled via the Shan and Chen multicomponent multiphase LB formulation [5]. The extra distribution function of the pseudotemperature is then coupled with flow at the macroscopic level via an EOS. In a broad sense, this is similar to the approach of [33], but there are important differences. In our approach, heats of reaction, latent heat associated with the phase change, reversible and irreversible conversion of mechanical energy to thermal energy, and external heat sources or sinks are readily included in the evolution equation for the extra distribution function.

This paper is organized as follows. The model formulation is presented in Sec. II, where we describe the proposed scheme to couple the Shan and Chen multiphase formulation with the energy equation. In Sec. III, we validate the method using two illustrative examples; here, for the sake of comparison with simple analytical solutions we limit ourselves to one-dimensional (1D) examples involving a single species (although we solve it as a 2D problem). However, it will be readily transparent that the scheme can be applied to multidimensional, multicomponent systems. The main conclusive remarks of this study are summarized in Sec. IV.

## II. NUMERICAL METHOD

In this section, we present the details of an approach based on the lattice Boltzmann method to solve the heat equation

*Corresponding author: m.r.kamali@tudelft.nl; mdrzkamali@gmail.com

 ©2013 American Physical Society

in two-phase systems. We first summarize the widely used Shan-Chen LB formulation for multicomponent two-phase flow. We then present an LB scheme to handle the transport of a scalar, which is specialized to capture the energy transport equation.

### A. Shan and Chen LB formulation for multicomponent two-phase hydrodynamics

Following Shan and Chen [5], the discrete LB-based evolution equation for the density distribution function of component $\delta$ in the lattice direction $i$, $f_{i,\delta}$, is written as

$$f_{i,\delta}(\mathbf{x}+\mathbf{c}_i,t+1)-f_{i,\delta}(\mathbf{x},t)=-\frac{f_{i,\delta}(\mathbf{x},t)-f_{i,\delta}^{eq}(\mathbf{x},t)}{\tau_\delta}. \quad (1)$$

This equation is written in terms of lattice variables, where length is scaled using the lattice spacing $\Delta x$, and time is made dimensionless using the time step $\Delta t$. Here, $\mathbf{c}_i$ is the (lattice) vector associated with the lattice direction $i$ (typically connecting the node $\mathbf{x}$ to a neighboring node when $i$ is not zero and equal to the null vector for $i=0$); $\tau_\delta$ is the relaxation time (in lattice units). The lattice speed $c_{\mathrm{ref}}=\Delta x/\Delta t$ is used to scale the velocities and obtain the corresponding lattice velocities; the speed of sound in lattice units, $c_s=1/\sqrt{3}$. The equilibrium distribution function is written as

$$f_{i,\delta}^{eq}(\mathbf{x},t) = w_i\rho_\delta\left\{1+\frac{\mathbf{c}_i\cdot\mathbf{u}_\delta^{eq}}{c_s^2}+\frac{1}{2}\left(\frac{\mathbf{c}_i\cdot\mathbf{u}_\delta^{eq}}{c_s^2}\right)^2-\frac{1}{2}\frac{\mathbf{u}_\delta^{eq}\cdot\mathbf{u}_\delta^{eq}}{c_s^2}\right\}. \quad (2)$$

Here, $w_i$ is the weight associated with direction $i$,

$$\rho_\delta=\sum_i f_{i,\delta},\quad \mathbf{u}_\delta^{eq}=\mathbf{u}'+\frac{\tau_\delta}{\rho_\delta}\sum_\delta \mathbf{F}_\delta^{\mathrm{tot}},$$
$$\mathbf{u}'=\sum_\delta\frac{\rho_\delta}{\tau_\delta}\mathbf{u}_\delta\Big/\sum_\delta\frac{\rho_\delta}{\tau_\delta},\quad \text{and}\quad \mathbf{u}_\delta=\frac{1}{\rho_\delta}\sum_i\mathbf{c}_i f_{\delta,i}. \quad (3)$$

In these equations, all quantities are in lattice units. The density $\rho$ in physical units is scaled by a reference density $\rho_{\mathrm{ref}}$ to convert to lattice units. The forcing term $\mathbf{F}_\delta^{\mathrm{tot}}=\mathbf{F}_\delta+\mathbf{F}_\delta^{\mathrm{ext}}$ includes the pseudopotential interaction force $\mathbf{F}_\delta$ between components occupying neighboring LB nodes and the external force $\mathbf{F}_\delta^{\mathrm{ext}}$. In general, $\mathbf{F}_\delta$ can be used to represent component-component as well as component-solid boundary interactions (e.g., see [17,35]). However, we consider only the former in the illustrative examples discussed in the present study. Following Shan and Chen [5]:

$$\mathbf{F}_\delta(\mathbf{x},t)=-\psi_\delta(\mathbf{x},t)\sum_{\bar\delta}G_{\delta\bar\delta}\sum_i w_i\psi_{\bar\delta}(\mathbf{x}+\mathbf{c}_i,t)\mathbf{c}_i, \quad (4)$$

where $G_{\delta\bar\delta}$ denotes the component-component interaction parameter and a suitable model for the pseudopotential function $\psi_\delta$ is postulated.

The illustrative example discussed later considers a single-component system following the Redlich-Kwong (RK) equation of state:

$$P_\delta c_s^{-2}=\frac{\rho_\delta\theta}{1-b_\delta\rho}-\frac{a_\delta\rho_\delta^2}{\sqrt{\theta}(1+b_\delta\rho_\delta)}. \quad (5)$$

Here, the temperature in physical units, $T$, has been scaled by $T_{\mathrm{ref}}$ to convert to the lattice temperature $\theta$; $\theta=T/T_{\mathrm{ref}}$. Similarly, the pressure is expressed in lattice units as $P_\delta=p_\delta/\rho_{\mathrm{ref}}c_{\mathrm{ref}}^2$ where $c_{\mathrm{ref}}^2=RT_{\mathrm{ref}}c_s^{-2}$ using the gas constant $R$. Following Yuan and Schafer [36], we write

$$\psi_\delta=\sqrt{\frac{P_\delta c_s^{-2}-\rho_\delta\theta}{\frac{1}{2}G_{\delta\delta}\theta}} \quad (6)$$

and set $G_{\delta\delta}=-1$, $a_\delta=2/49$, and $b_\delta=2/21$. These correspond to the following critical state parameters in lattice units: $P_{c\delta}=0.1785c_s^2=0.0595$, $\theta_{c\delta}=0.1961$, and $\rho_{c\delta}=2.73$. The kinematic viscosity of species $\delta$ (in lattice units), $\nu_\delta$, is given by $\nu_\delta=(\tau_\delta-0.5)/3$.

In brief, the density field in Eq. (1) is affected by the temperature field through the EOS and by the corresponding variables calculated in Eqs. (2)–(6).

### B. Energy balance equation

It can readily be shown that the general balance equations for species and energy in a multicomponent system take the following form [37]:

$$\frac{\partial\rho_\delta}{\partial t}+\nabla\cdot\mathbf{n}_\delta=r_\delta, \quad (7)$$

$$\frac{\partial}{\partial t}\left(\sum_\delta\rho_\delta\overline{H}_\delta\right)+\nabla\cdot\left(\sum_\delta\mathbf{n}_\delta\bar H_\delta\right) = \nabla\cdot(K\nabla T)+\frac{DP}{Dt}+\hat\tau:\nabla\mathbf{v}+\sum_\delta\mathbf{j}_\delta\cdot\mathbf{B}_\delta+Q^\bullet. \quad (8)$$

In the species balance, $\mathbf{n}_\delta$ and $r_\delta$ denote the flux and rate of generation (via chemical reactions) of component $\delta$. $DP/Dt$, $\hat\tau$, and $Q^\bullet$ are the pressure gradient, stress tensor, and external heat rate per unit volume, respectively. $\bar H_\delta(\rho,T)$, the partial specific enthalpy for component $\delta$ (appearing in the energy balance), is in general a function of temperature, pressure, and composition; however, in most practical applications, the dependence of $\bar H_\delta$ in a given phase on pressure and composition is only weak (when compared to the enthalpy changes associated with progress in the reaction extent and/or phase change). In what follows, we make this simplification. With this restriction, we write

$$\bar H_\delta(\rho,T)=[1-\phi(\rho)]\bar H_\delta^v(T)+\phi(\rho)\bar H_\delta^l(T). \quad (9)$$

Here, $\bar H_\delta^v(T)$and $\bar H_\delta^l(T)$ are the partial specific enthalpies for component $\delta$ in the vapor and the liquid phases at temperature $T$, respectively. $\rho=\sum_\delta\rho_\delta$ is the mixture density. $\phi(\rho)$ is a (user-specified) density-dependent marker function such that it assumes a value of 0 in the bulk vapor and unity in the bulk liquid and increases monotonically with density in between. For example, a piecewise linear model would take the form

$$\phi(\rho)=\begin{cases}0, & \rho<\rho_1,\\ \frac{\rho-\rho_1}{\rho_2-\rho_1}, & \rho_2>\rho>\rho_1,\\ 1, & \rho>\rho_2.\end{cases} \quad (10)$$

Here, $\rho_2$ and $\rho_1$ are user-specified threshold mixture densities which are used to identify the phase of the mixture. When the mixture density is below $\rho_1$, it is treated as a gas (vapor); similarly, when it is larger than $\rho_2$, it is treated as a liquid phase. When $\rho$ is in between these two, the property of interest (such as the partial specific enthalpy) is suitably interpolated.

It is clear that the principal purpose of Eq. (9) is to provide estimates for enthalpy in the diffuse interface region. The specific choice of $\phi(\rho)$ will affect the details of the profiles in the interfacial region, but will have little effect in the bulk regions far away from the interface. For later use, we note that

$$\Delta\bar{H}_\delta^{lv}(T) = \bar{H}_\delta^{v}(T) - \bar{H}_\delta^{l}(T) \tag{11}$$

is the latent heat of vaporization at that temperature.

The heat capacity of the component $\delta$ is interpolated in an analogous manner:

$$C_{p,\delta}(T) = (1-\phi(\rho))C_{p,\delta}^{v}(T) + \phi(\rho)C_{p,\delta}^{l}(T) \tag{12}$$

It makes physical sense to use the same marker function for both enthalpy and heat capacity, but the error introduced by using different marker functions for enthalpy and heat capacity will invariably be small (as the mass of material in the "diffuse" interfacial region is usually much smaller than that in the bulk).

To follow up with the description of the terms in the energy balance equation (8), $K = \sum_\delta \rho_\delta K_\delta/\rho$ is the thermal conductivity of the mixture. The third and fifth terms on the right-hand side of the energy balance equation (8) represents the rates of viscous generation of heat and external heat input (per unit volume), respectively. The fourth term denotes the rate of work done by the external (body) force on the diffusive fluxes of various species; $\mathbf{B}_\delta$ denotes the external force per unit mass acting on component $\delta$, and $\mathbf{j}_\delta$ is the diffusive flux of component $\delta$,

$$\mathbf{j}_\delta = \mathbf{n}_\delta - \rho_\delta \mathbf{v}. \tag{13}$$

The mixture velocity is defined by $\mathbf{v} = \sum_\delta \mathbf{n}_\delta/\rho$. When the external force per unit mass is the same for all the species, $\sum_\delta \mathbf{j}_\delta \cdot \mathbf{B}_\delta = 0$.

It is straightforward to rewrite the energy balance and the above restrictions to get

$$\frac{\partial T}{\partial t} + \mathbf{v}\cdot\nabla T = \frac{\nabla\cdot(K\nabla T)}{\sum_\delta \rho_\delta C_{p,\delta}} + \frac{S}{\sum_\delta \rho_\delta C_{p,\delta}}, \tag{14}$$

where the source term $S$ is given by

$$\begin{aligned} S = &-\sum_\delta r_\delta \bar{H}_\delta + \left(\sum_\delta \rho_\delta \Delta\bar{H}_\delta^{lv}\right)\phi'(\rho)\frac{D\rho}{Dt} \\ &- \left(\sum_\delta \mathbf{j}_\delta C_{p,\delta}\right)\cdot\nabla T + \left(\sum_\delta \mathbf{j}_\delta \Delta\bar{H}_\delta^{lv}\right)\cdot\phi'(\rho)\nabla\rho \\ &+ \frac{DP}{Dt} + \hat{\tau}:\nabla\mathbf{v} + \sum_\delta \mathbf{j}_\delta\cdot\mathbf{B}_\delta + Q^\bullet. \end{aligned} \tag{15}$$

In what follows, we present a lattice Boltzmann scheme to solve Eq. (14). In preparation for that, we first cast Eqs. (14) and (15) into dimensionless form (using the same scales as used in defining lattice units) using $\Delta x$, $\Delta t$, $c_{\rm ref} = \Delta x/\Delta t$, $\rho_{\rm ref}, T_{\rm ref}$, $p_{\rm ref} = \rho_{\rm ref}c_{\rm ref}^2$, $C_{p,\rm ref}$, and $C_{p,\rm ref}T_{\rm ref}$ as the reference length, time, velocity, density, temperature, pressure, heat capacity, and enthalpy per unit mass. The reference thermal conductivity, viscosity, diffusive flux, reaction rate, and external heat source [corresponding to the last term on the right-hand side of Eq. (15)] are set as $\rho_{\rm ref}C_{p,\rm ref}\Delta x^2/\Delta t$, $\rho_{\rm ref}\Delta x^2/\Delta t$, $\rho_{\rm ref}c_{\rm ref}$, $\rho_{\rm ref}/\Delta t$, and $\rho_{\rm ref}C_{p,\rm ref}T_{\rm ref}/\Delta t$, respectively. The resulting dimensionless equations will be the same as Eqs. (14) and (15), except that we now recognize all the variables as scaled quantities (with the scaled $T$ being the same as $\theta$ in the earlier section).

The scaled equations now read

$$\frac{\partial\theta}{\partial t} + \mathbf{v}\cdot\nabla\theta = \frac{\nabla\cdot K\nabla\theta}{\sum_\delta \rho_\delta C_{p\delta}} + \frac{S}{\sum_\delta \rho_\delta C_{p\delta}}, \tag{16}$$

$$\begin{aligned} S = &-\sum_\delta r_\delta \bar{H}_\delta + \left(\sum_\delta \rho_\delta \Delta\bar{H}_\delta^{lv}\right)\phi'(\rho)\frac{D\rho}{Dt} \\ &- \left(\sum_\delta \mathbf{j}_\delta C_{p,\delta}\right)\cdot\nabla\theta + \left(\sum_\delta \mathbf{j}_\delta \Delta\bar{H}_\delta^{lv}\right)\cdot\phi'(\rho)\nabla\rho \\ &+ \left(\frac{R}{C_{p,\rm ref}c_s^2}\right)\left(\frac{DP}{Dt} + \hat{\tau}:\nabla\mathbf{v} + \sum_\delta \mathbf{j}_\delta\cdot\mathbf{B}_\delta\right) + Q^\bullet. \end{aligned} \tag{17}$$

Here, we have retained the same symbols to indicate scaled variables; in what follows, we consider only scaled quantities and so there should be no confusion. Although we could have chosen $C_{p,\rm ref} = R/c_s^2$, we chose not to make this restriction as the contribution from $(\frac{DP}{Dt} + \hat{\tau}:\nabla\mathbf{v} + \sum_\delta \mathbf{j}_\delta\cdot\mathbf{B}_\delta)(R/C_{p,\rm ref}c_s^2)$ is expected to be quite small in most flow problems.

### C. LB formulation for the energy balance equation

We introduce a distribution function $g$ for a pseudotemperature scalar such that

$$\rho\theta = \sum_i g_i \tag{18}$$

and evolve it using

$$g_i(\mathbf{x}+\mathbf{c}_i, t+1) - g_i(\mathbf{x},t) = -\frac{g_i - g_i^{eq}}{\tau_H} + w_i S^{LB}. \tag{19}$$

Here $\tau_H$ is the relaxation time for the pseudotemperature scalar variable, and its equilibrium distribution function is defined as

$$g_i^{eq} = w_i\rho\theta\{1 + 3\mathbf{c}_i\cdot\mathbf{v}\} \tag{20}$$

and $\mathbf{v}$, the macroscopic velocity, is defined as [38]

$$\mathbf{v} = \frac{1}{\rho}\sum_\delta\sum_i \mathbf{c}_i f_{i,\delta} + \frac{1}{2\rho}\sum_\delta \mathbf{F}_\delta. \tag{21}$$

One can readily show via a Chapman-Enskog or multiscale expansion [39] that solving these microscopic equations is equivalent to solving

$$\rho\frac{\partial\theta}{\partial t} + \rho\mathbf{v}\cdot\nabla\theta = \nabla\cdot[\alpha^{LB}\nabla(\rho\theta)] + S^{LB}, \tag{22}$$

where the lattice thermal diffusivity $\alpha^{LB} = (\tau_H - 0.5)/3$. Comparing Eqs. (16) and (22), we identify $S^{LB}$ as

$$S^{LB} = \frac{S}{C_{p,\rm mix}} + \frac{\nabla\cdot(K\nabla\theta)}{C_{p,\rm mix}} - \nabla\cdot[\alpha^{LB}\nabla(\rho\theta)], \tag{23}$$

where the heat capacity of the mixture $C_{p,\rm mix} = \sum_\delta \rho_\delta C_{p,\delta}/\rho$. Equation (23) can be rearranged to read

$$S^{LB} = \sum_{n=1}^{10} S_n^{LB}, \tag{24}$$

where

$$S_1^{LB} = -\sum_\delta r_\delta \bar{H}_\delta / C_{p,\mathrm{mix}},$$

$$S_2^{LB} = \left(\sum_\delta \rho_\delta \Delta \bar{H}_\delta^{lv} \phi'(\rho) \frac{D\rho}{Dt}\right) \Big/ C_{p,\mathrm{mix}},$$

$$S_3^{LB} = -\left(\sum_\delta \mathbf{j}_\delta C_{p,\delta}\right) \cdot \nabla\theta / C_{p,\mathrm{mix}},$$

$$S_4^{LB} = \left(\sum_\delta \mathbf{j}_\delta \Delta \bar{H}_\delta^{lv}\right) \cdot \phi'(\rho) \nabla\rho / C_{p,\mathrm{mix}},$$

$$S_5^{LB} = R\left(\frac{DP}{Dt}\right) \Big/ \left(C_{p,\mathrm{mix}} C_{p,\mathrm{ref}} c_s^2\right),$$

$$S_6^{LB} = R(\hat{\tau} : \nabla \mathbf{v}) / \left(C_{p,\mathrm{mix}} C_{p,\mathrm{ref}} c_s^2\right),$$

$$S_7^{LB} = R\left(\sum_\delta \mathbf{j}_\delta \cdot \mathbf{B}_\delta\right) \Big/ \left(C_{p,\mathrm{mix}} C_{p,\mathrm{ref}} c_s^2\right),$$

$$S_8^{LB} = Q^\bullet / C_{p,\mathrm{mix}},$$

$$S_9^{LB} = \nabla \cdot (K \nabla\theta) / C_{p,\mathrm{mix}},$$

$$S_{10}^{LB} = -\nabla \cdot [\alpha^{LB} \nabla(\rho\theta)].$$

In most reacting flows, we expect $S_5^{LB} \approx 0$, $S_6^{LB} \approx 0$, and $S_8^{LB} = 0$.

## III. RESULTS AND DISCUSSION

Although the model is set up for a multicomponent system, it suffices to examine a single-component system to validate it. For a single-component system, $S_1^{LB} = S_3^{LB} = S_4^{LB} = 0$. This simplification does not eliminate the complexity of the model as many other source terms (e.g., that related to phase change) still remain. When dealing with single-component systems, there is no need for the component index $\delta$ and so it is suppressed in the material below.

As mentioned earlier, in our illustrative examples discussed below, the fluid is assumed to follow the Redlich-Kwong EOS. For the parameter values listed below Eq. (6), one obtains $\theta_c = 0.1961$ and $\rho_c = 2.73$. In these examples, for $\theta < \theta_c$, the system will undergo phase separation and form a two-phase mixture; the densities of the saturated vapor and liquid phases can readily be found by solving the LB evolution equations. One can also find them via Maxwell's equal area construction. The saturated vapor and liquid densities determined via LB simulations are compared with those obtained via a Maxwell construction in Fig. 1. Good agreement is readily seen over the range of $\theta_R = \theta/\theta_c$ values shown there. The liquid and vapor densities reported in this figure are used in the following examples.

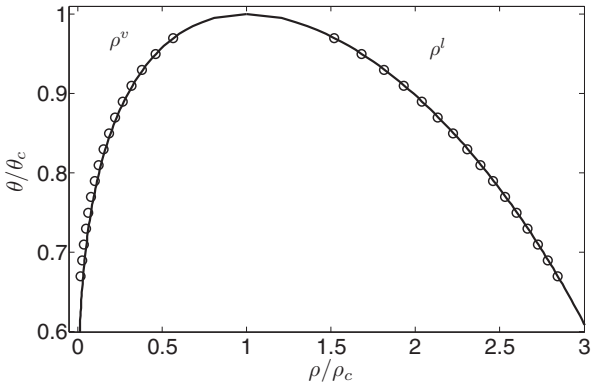


FIG. 1. Liquid and vapor density variations with temperature for the RK EOS. Solid line, theoretical values obtained from the Maxwell rule of equal areas; markers, LB simulations obtained from the Shan and Chen formulation.

### A. Example 1: One-dimensional heat transport through a liquid-vapor flat interface

In this example, we simulated one-dimensional nonevaporative heat conduction in a system containing a single planar vapor-liquid interface, which was located in the gap between two parallel walls (and was also parallel to the walls). All quantities are in lattice units and unless stated otherwise, $\Delta z = 1$, $\Delta t = 1$ (also in lattice units). (Here, the $z$ axis is pointing perpendicular to the walls.) The Zou and He approach [40] was used to implement the thermal boundary conditions on the walls. The system was initially allowed to equilibrate at a uniform reduced temperature $\theta_{R0} = \theta_0/\theta_c = 0.75$ and form the vapor-liquid interface as mentioned above. At equilibrium, $\rho^l/\rho_c = 2.6$ and $\rho^v/\rho_c = 0.0618$ (see Fig. 1). The location of the interface depended on the mass of material that was placed in the gap, and, in this specific instance, the stationary vapor-liquid interface was established at $h/L = 0.55$. Here, $L$ is the gap width and $h$ is the approximate location of the interface. In the numerical example presented here, $L = 100$. In this one-component two-phase system, the thickness of the vapor-liquid interface was between 3 and 7 (in lattice units). (The interface thickness decreased upon lowering the temperature.) After allowing the system to equilibrate, the wall temperatures were changed and the routine for solving the LB energy equation was switched on. Specifically, the temperature of the left wall (in contact with the vapor phase) was increased to $\theta_1$ while that of the right wall (in contact with the liquid phase) was maintained at $\theta_2 = \theta_0$, $\theta_1$ being slightly larger than $\theta_2$. In general, temperature changes would be accompanied by a phase change, but in this simple example, we *disallowed* phase change. This was achieved in the simulations by simply letting the temperature appearing in the EOS remain at $\theta_0$. Heat was still transmitted from the hotter wall to the colder wall, across the liquid-vapor interface; and we tested the adequacy of LB scheme for handling heat transfer in the presence of an interface.

In this test example, the kinematic viscosities of the vapor and liquid phases were assigned the same value $\nu^l = \nu^v = 1/6$. We set the Prandtl number in the vapor $\mathrm{Pr}^v = \nu^v/\alpha^v = 1$ and the one in the liquid $\mathrm{Pr}^l = \nu^l/\alpha^l = 5$, which led to $\alpha^v = 1/6$ and $\alpha^l = 1/30$. The thermal diffusivities were used to calculate the source contribution $S_9^{LB}$ in Eq. (24). The pseudotemperature relaxation time $\tau_H$ was assigned a value very close to 0.5 in order to minimize the contribution from the last term on the right-hand side of Eq. (23), which has to be explicitly subtracted out through the term $S_{10}^{LB}$ in Eq. (24) [33]. (In this example, $S_9^{LB}$ and $S_{10}^{LB}$ are the only nonzero source terms.) The heat capacities of the vapor and liquid phases

TABLE I. Physical properties of liquid and vapor phases using the RK EOS at $\theta_{R0} = 0.75$ with $\mathrm{Pr}^l = 5$ and $\mathrm{Pr}^v = 1$. (Note: All quantities are in lattice units.)

| Property | $\rho^l/\rho_c$ | $\rho^v/\rho_c$ | $\rho^l/\rho^v$ | $\alpha^l$ | $\alpha^v$ | $\alpha^l/\alpha^v$ | $C_p^l$ | $C_p^v$ | $C_p^l/C_p^v$ | $K^l/\rho_c$ | $K^v/\rho_c$ | $K^l/K^v$ |
|---|---|---|---|---|---|---|---|---|---|---|---|---|
| | 2.60 | 0.0618 | 42.07 | 1/30 | 1/6 | 0.20 | 2.62 | 2.5 | 1.05 | 0.227 | 0.0258 | 8.8 |

were calculated from the EOS [20] at $\theta_0$, although the scheme does not require that the heat capacities be calculated in this manner. All of these parameters were then used to calculate the thermal conductivities of the two phases at $\theta_0$. Table I summarizes the physical properties of the bulk fluids.

In addition to the values of the thermal conductivity $K$ in the bulk liquid and vapor phases (see Table I), the density dependence of $K$ in the interfacial region must also be postulated. We demand $dK/d\rho = d(\rho C_p \alpha)/d\rho > 0$ (in order to avoid unphysical behavior). For example, one can satisfy this requirement by letting $\alpha(z) = \varepsilon_1(\rho(z))^{\beta_1}$ and $C_p(z) = \varepsilon_2(\rho(z))^{\beta_2}$ with $1 + \beta_1 + \beta_2 > 0$. We set $\alpha(z) = 0.0776\rho^{-0.43}$ and $C_p(z) = 2.56\rho^{0.01}$. Figure 2 shows the spatial variation of various physical properties for this example. The LB equation for the pseudotemperature was then solved until a steady state was attained. An analytical solution for this problem involving heat conduction in a two-layered material is readily found; the steady-state temperature profile in either layer is linear. For convenience, we define $\hat{\theta} = 1 + (\theta - \theta_2)/(\theta_1 - \theta_2)$ and display the steady-state profile of temperature scaled in such a manner. Figure 3 compares the steady-state temperature field obtained from the LB simulations (shown by open circles) with the analytical solution for a system with a sharp interface (shown by solid line). The accuracy of the simulation results was assessed by calculating the error $\in$ between the analytical (AN) results and LB simulations over the entire domain ($iz = 1$–$n_z$):

$$\in = \sqrt{\sum_{iz} [\theta^{LB}(iz) - \theta^{AN}(iz)]^2} \Big/ \sqrt{\sum_{iz} [\theta^{AN}(iz)]^2}. \quad (25)$$

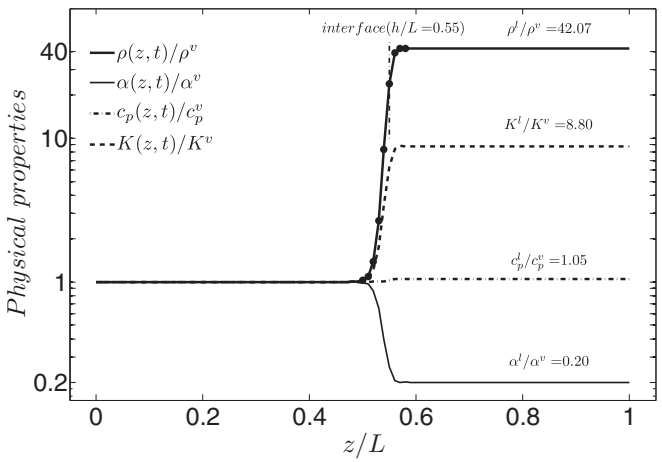


FIG. 2. Scaled density (thick solid line), scaled thermal diffusivity (thin solid line), scaled thermal conductivity (dashed line), and scaled heat capacity (dash-dotted line) as functions of the coordinate normal to a gas-liquid interface.

The inset of Fig. 3 reveals that the accuracy of the current formulation depends on the relaxation times $\tau_H$; the accuracy is improved as $\tau_H$ is decreased towards the minimum permissible limit of 0.5. Equivalently, to get the best accuracy, $\alpha^{LB}$ should be set to be very close to zero. This rather simple example illustrates that the vapor-liquid interfacial region where the physical properties change rapidly does not cause any computational difficulty and that the expected analytical solution is recovered.

In this example, the temperature field was deliberately *not* coupled to the hydrodynamics, i.e., while the temperature field evolved towards steady state, the density and velocity fields remained invariant. Next we consider an example where local temperatures are coupled back in the EOS, so that the density and velocity fields will also evolve while the temperature field develops; the phase interface is now dynamic as evaporation and condensation can occur.

### B. Example 2: Evaporation of a liquid film upon heating

In this example, we assess the accuracy of the proposed LB scheme when evaporation occurs as a result of heating. We consider the response of a single-component system obeying the Redlich-Kwong EOS to a constant uniform heat input. Figure 4 illustrates the state of a system initially equilibrated at a homogeneous reduced temperature $\theta_{R0} = 0.75$. In this example, the total length of the domain $L = 200$ (lattice units), and the liquid layer occupies approximately 40% of the domain. At the two ends, we applied periodic boundary conditions. (Adiabatic wall boundary conditions would have

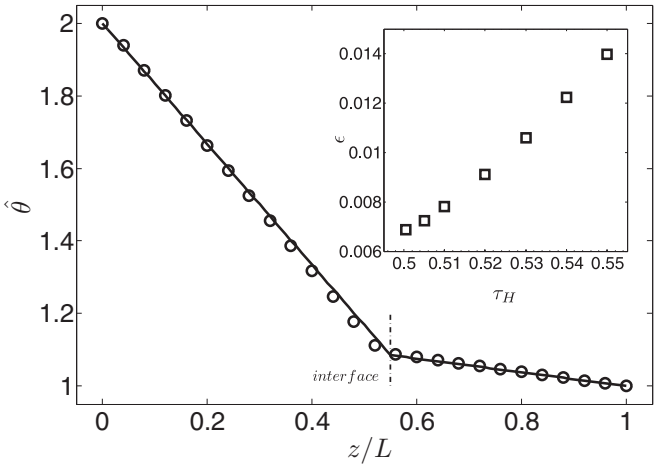


FIG. 3. Steady-state temperature obtained for Example 1 from LB-based model (circles) compared with the analytical solution (line) for the one-dimensional thermal diffusion problem. Inset: Error $\in$ between LB simulation results and the exact solution at various relaxation times $\tau_H$.

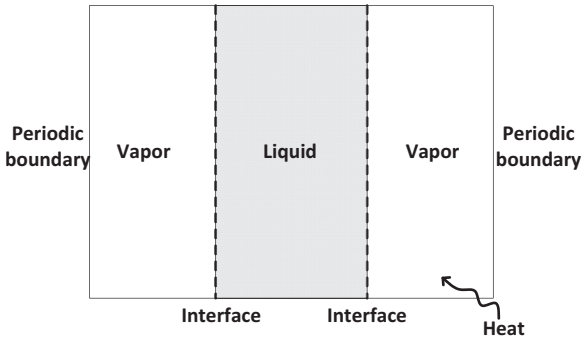


FIG. 4. Schematic representation of Example 2 involving evaporation in 1D. A two-phase system as shown in the figure is exposed to uniform heating, which causes vaporization of the liquid. As periodic boundary conditions are employed in these simulations, the total mass is conserved; so vaporization is accompanied by an increase in the vapor phase density (and pressure).

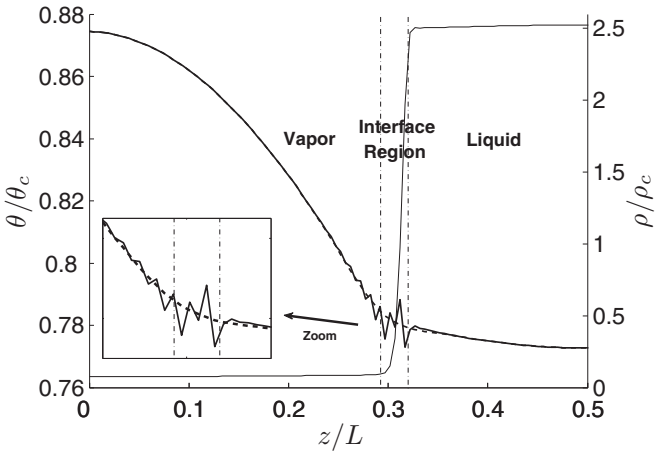


FIG. 5. Density profile (thin solid line read from right $y$ axis), temperature profile (thick solid line read from left $y$ axis), and the smoothed temperature profile used in the EOS (broken line read from left $y$ axis) at $\tilde{t} = 0.03$ in Example 2. Only one-half of the domain is shown; the other half of the domain is simply a mirror image of the region shown. A two-phase system is exposed to uniform heating, which causes vaporization of the liquid (see Fig. 4 for a schematic). The vapor heats up faster as its density is lower than that of the liquid and the heating rate per volume is uniform in this example. Inset: Zoom of temperature close to the diffused interface region.

led to the same results.) The physical properties reported in Table I were used. The temperature and phase densities evolved with time, and so did some of the physical properties such as heat capacity (although, small variations in the course of this numerical experiment were observed) and thermal conductivity.

The following procedure allowed us to establish efficiently the initial condition for the transient heating simulations. The LB evolution equations for the species and the pseudotemperature were solved towards steady state first without coupling them through the EOS; then the coupling between the energy equation and hydrodynamics via the EOS was turned on and the system was allowed to equilibrate. The system was then subjected to uniform heating. This heat flux ($Q^{\bullet} = 10^{-6}$) and the enthalpy of the phase change ($\overline{\Delta H}^{lv} = 0.5$) entered in the simulation via the local source terms in Eq. (24), $S_8^{LB}$ and $S_2^{LB}$, respectively. With a spatially uniform heat source (fixed rate of heat addition per unit volume), one can readily expect the vapor to heat up faster than the liquid. As the system heated up, vaporization occurred, resulting in a movement of the vapor-liquid interface. It was found in the simulations that the pseudotemperature variable manifested small fluctuations in the vicinity of the phase interface, and that these fluctuations could sometimes destabilize the computations. These fluctuations mainly originate from the density variation along the diffused interface. In order to avoid such instabilities, the local temperature field close to the interface at each time step was smoothed (the smoothing parameter is 100) using a regularized robust spline algorithm due to Garcia [41]. Figure 5 illustrates temperature filtering at a certain instance of time of the simulation. As no mass leaves the system (due to the periodic boundary conditions), the vapor density increased with time as result of evaporation, and so did the pressure in the computational domain. When the system temperature reached the critical point, the phase interface disappeared, as one would expect. We present only results from before the critical point was reached, as our primary intention is to demonstrate that the proposed LB scheme works well for two-phase systems.

Figure 6 shows the LB simulation results for the unfiltered temperature profiles at different dimensionless times $\tilde{t} = t\,Q^{\bullet}/(\rho_c C_p^l \theta_c)$. At $\tilde{t} = 0$, the system was at a uniform temperature $\theta_{R0} = 0.75$. Starting up the simulations at lower initial temperature than the ones reported in this example may be possible by improving the explicit pseudopotential interparticle interactions in the Shan and Chen approach as reported by Kupershtokh *et al.* [42]. Filtering is not found to be influential in this respect. The nearly parabolic profile in the gas phase can readily be understood, as the quasisteady limit for the temperature profile is indeed a parabola with

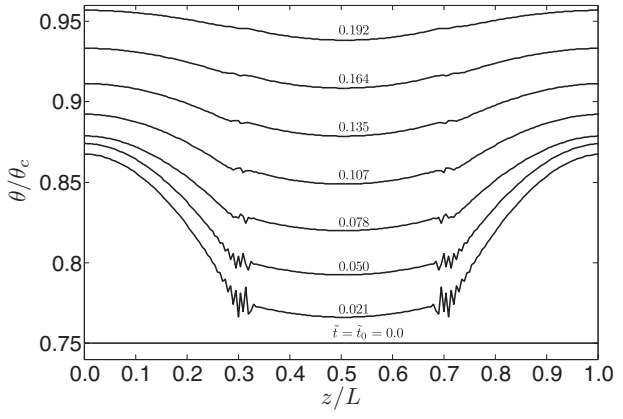


FIG. 6. Temperature profiles at various dimensionless times in Example 2. A two-phase system is exposed to uniform heating, which causes vaporization of the liquid (see Fig. 4 for a schematic). The vapor heats up faster as its density is lower than that of the liquid and the heating rate per volume is uniform in this example. The pure substance considered in this example obeys the Redlich-Kwong equation of state.

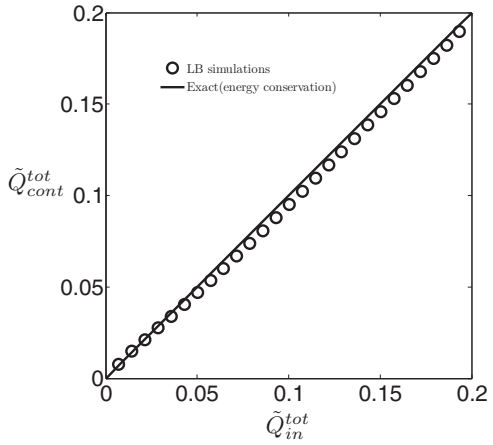


FIG. 7. Comparison between LB simulations and exact solution for total heat input vs total heat contained in the system in Example 2. A two-phase system is exposed to uniform heating, which causes vaporization of the liquid (see Fig. 4 for a schematic). The pure substance considered in this example obeys the Redlich-Kwong equation of state. The total heat contained in the system was found by integrating (over the domain). The parity plot shows that the evolution of the LB distribution functions for the species and pseudotemperature are correctly coupled with the equation of state. The maximum relative error throughout the simulation is 7%.

time-dependent coefficients. The nearly flat temperature of the liquid phase can be traced to its high thermal conductivity. As more and more vaporization occurs, the densities of the two phases approach each other and the temperatures in the two phases approach one another.

The total amount of heat supplied to the system clearly increased linearly with time and is trivially computed from the specified heating rate. This allowed us to check the accuracy of the LB scheme by determining the total enthalpy of the system as a function of time. For this calculation, we set the specific enthalpy of the liquid at the reference temperature $\theta_0$ to zero: $\overline{H}^l(\theta_0) = 0$. Thus, the enthalpy of the vapor at this temperature is the latent heat of vaporization $\overline{H}^v(\theta_0) = \overline{\Delta H}^{lv}(\theta_0)$. The specific enthalpies of the bulk liquid and vapor at different temperatures were then calculated from

$$\overline{H}^l(\theta) = \int_{\theta_0}^{\theta} C_P^l d\theta, \quad \overline{H}^v(\theta) = \overline{\Delta H}^{lv}(\theta_0) + \int_{\theta_0}^{\theta} C_P^v d\theta. \tag{26}$$

Then, by using the marker function $\phi(\rho)$ in Eq. (10), the specific enthalpy at any intermediate density $\overline{H}(\rho,\theta)$ was captured via Eq. (9). A mass-weighted sum of $\overline{H}(\rho,\theta)$ over the whole domain yielded the total enthalpy of the system at any time $Q^{\text{tot}}_{\text{cont}}$.

Figure 7 compares the dimensionless total heat input to the domain $\tilde{Q}^{\text{tot}}_{in} = Q^{\text{tot}}_{in}/(\rho_c C^l_p \theta_c L)$ and the computed dimensionless total enthalpy of the system $\tilde{Q}^{\text{tot}}_{\text{cont}} = Q^{\text{tot}}_{\text{cont}}/(\rho_c C^l_p \theta_c L)$. This comparison shows a maximum 7% error between the numerical LB results and the theory throughout the simulation. This good agreement shows that the proposed LB scheme for the coupling between the pseudotemperature and the hydrodynamics via the EOS correctly captures the energies associated with the phase change.

## IV. CONCLUSIONS

A lattice Boltzmann method is presented for dealing with heat transport in two-phase systems with the ability of incorporating phase change phenomena. This approach employs multiple distribution functions, one for a pseudotemperature variable and the rest for various species. A nonideal equation of state is introduced by using the Shan and Chen method [5].

Starting from the well-known macroscopic energy conservation equation for mixtures, we first constructed the continuum limit of the LB evolution equation for the pseudotemperature variable. Using this limit as the guide, the LB evolution equations were then formulated. In the proposed scheme, heats of reaction, the enthalpy change associated with the phase change, and diffusive transport of enthalpy are all readily taken into account. However, the dependence of enthalpy on pressure has been ignored. In most chemically reacting flows encountered in chemical industries, the pressure dependence of enthalpy contributes very little to the evolution of the temperature field and therefore this simplification is not a serious limitation. (If the pressure dependence is important in a given problem, improvements to the present model will be needed.)

As in other numerical schemes, such as the volume of fluid method, the vapor-liquid interface in the LB simulations is more diffuse than in real systems. As a result, one has to postulate how physical properties vary with density across the diffuse interface; any postulate one makes about this variation is only an approximation. We present a simple model based on marker functions. The details of the variations in the diffuse interface will necessarily depend on the choice of marker functions; however, as the amount of material in this diffuse interface is small compared to the total mass in the system, the overall influence of the choice of marker functions is generally insignificant.

The energy equation is coupled to the LB equations for species transport through the EOS. We found that the computed (pseudo)temperature field in the vicinity of the diffuse interface manifested noisy fluctuations, which under some conditions caused the coupled scheme to be unstable. This problem was easily removed by employing in the EOS a filtered temperature field obtained by using a regularized robust spline algorithm due to Garcia [41]. Furthermore, the thermal boundary conditions were implemented following the model proposed by Zou and He [40].

The proposed scheme was validated against several simple test problems, two of which are illustrated in this article. The first example considered a case where the temperature field was *not* coupled to the EOS. This example demonstrated that heat conduction across the vapor-liquid interface when the liquid and vapor physical and thermal properties are very close to the values in the real systems could be handled without any problem.

The second example allowed for coupling of the EOS with the energy equation and examined heating of a two-phase mixture. The heat source appeared in the energy balance,

which altered the temperature field; the EOS then dictated if and where phase change should occur; the phase change led to species transport and a change in the temperature field. We demonstrated that the proposed scheme correctly captured a readily verifiable macroscopic quantity, namely, the enthalpy content in the system. In our opinion, the proposed scheme can be used to simulate nonisothermal multiphase reacting flows, which are encountered widely in chemical industries.

## ACKNOWLEDGMENTS

The financial support of the Dutch Technology Foundation STW, the Applied Science Division of the Netherlands Organization for Scientific Research (NWO), is highly appreciated. M.R.K. would like to also thank the Islamic Development Bank for support via a scholarship through the Merit Scholarship Program for High Technology.

[1] R. Scardovelli and S. Zaleski, Annu. Rev. Fluid Mech. **31**, 567 (1999).
[2] G. Tryggvason, B. Bunner, A. Esmaeeli, D. Juric, N. Al-Rawahi, W. Tauber, J. Han, S. Nas, and Y. J. Jan, J. Comput. Phys. **169**, 708 (2001).
[3] N. G. Deen, M. van Sint Annaland, and J. A. M. Kuipers, Chem. Eng. Sci. **59**, 1853 (2004).
[4] J. A. Sethian and P. Smereka, Annu. Rev. Fluid Mech. **35**, 341 (2003).
[5] X. Shan and H. Chen, Phys. Rev. E **47**, 1815 (1993).
[6] A. K. Gunstensen, D. H. Rothman, S. Zaleski, and G. Zanetti, Phys. Rev. A **43**, 4320 (1991).
[7] X. Shan and H. Chen, Phys. Rev. E **49**, 2941 (1994).
[8] M. R. Swift, W. R. Osborn, and J. M. Yeomans, Phys. Rev. Lett. **75**, 830 (1995).
[9] M. R. Swift, E. Orlandini, W. R. Osborn, and J. M. Yeomans, Phys. Rev. E **54**, 5041 (1996).
[10] L. S. Luo, Phys. Rev. Lett. **81**, 1618 (1998).
[11] X. He, S. Chen, and R. Zhang, J. Comput. Phys. **152**, 642 (1999).
[12] K. Sankaranarayanan, X. Shan, I. G. Kevrekidis, and S. Sundaresan, Chem. Eng. Sci. **54**, 4817 (1999).
[13] A. J. Wagner and J. M. Yeomas, Phys. Rev. E **59**, 4366 (1999).
[14] K. Sankaranarayanan, X. Shan, I. G. Kevrekidis, and S. Sundaresan, J. Fluid Mech. **452**, 61 (2002).
[15] M. Sbragaglia, R. Benzi, L. Biferale, S. Succi, K. Sugiyama, and F. Toschi, Phys. Rev. E **75**, 026702 (2007).
[16] M. Sbragaglia, R. Benzi, L. Biferale, H. Chen, X. Shan, and S. Succi, J. Fluid Mech. **628**, 299 (2009).
[17] M. R. Kamali, J. J. J. Gillissen, S. Sundaresan, and H. E. A. Van den Akker, Chem. Eng. Sci. **66**, 3452 (2011).
[18] J. Zhang, Microfluid. Nanofluid. **10**, 1 (2011).
[19] M. R. Kamali, S. Sundaresan, H. E. A. Van den Akker, and J. J. J. Gillissen, Chem. Eng. J. **207-208**, 587 (2012).
[20] M. R. Kamali, Ph.D. thesis, Delft University of Technology, Delft, Netherlands, 2013.
[21] F. J. Alexander, S. Chen, and J. D. Sterling, Phys. Rev. E **47**, R2249 (1993).
[22] Y. H. Qian, J. Sci. Comput. **8**, 231 (1993).
[23] T. Seta, K. Kono, and S. Chen, Int. J. Mod. Phys. B **17**, 169 (2003).
[24] G. Gonnella, A. Lamura, and V. Sofonea, Phys. Rev. E **76**, 036703 (2007).
[25] B. J. Palmer and D. R. Rector, Phys. Rev. E **61**, 5295 (2000).
[26] R. Zhang and H. Chen, Phys. Rev. E **67**, 066711 (2003).
[27] B. J. Palmer and D. R. Rector, Phys. Rev. E **69**, 049903 (2004).
[28] G. Gonnella, A. Lamura, A. Piscitelli, and A. Tiribocchi, Phys. Rev. E **82**, 046302 (2010).
[29] G. Gonnella, A. Lamura, and A. Tiribocchi, Philos. Trans. R. Soc., A **369**, 2592 (2011).
[30] X. Shan, Phys. Rev. E **55**, 2780 (1997).
[31] X. He, S. Chen, and G. D. Doolen, J. Comput. Phys. **146**, 282 (1998).
[32] P. Yuan and L. Schaefer, J. Fluids Eng. **128**, 142 (2006).
[33] A. Márkus and G. Házi, Phys. Rev. E **83**, 046705 (2011).
[34] L. Biferale, P. Perlekar, M. Sbragaglia, and F. Toschi, Phys. Rev. Lett. **108**, 104502 (2012).
[35] M. R. Kamali and H. E. A. Van den Akker, Ind. Eng. Chem. Res. **52**, 11365 (2013).
[36] P. Yuan and L. Schaefer, Phys. Fluids **18**, 042101 (2006).
[37] W. Deen, *Analysis of Transport Phenomena* (Oxford University Press, New York, 1998).
[38] X. Shan and G. Doolen, J. Stat. Phys. **81**, 379 (1995).
[39] D. Wolf-Gladrow, *Lattice-Gas Cellular Automata and Lattice Boltzmann Models: An Introduction* (Springer, New York, 2000).
[40] Q. Zou and X. He, Phys. Fluids **9**, 1591 (1997).
[41] D. Garcia, Comput. Stat. Data Anal. **54**, 1167 (2010).
[42] A. L. Kupershtokh, D. A. Medvedev, and D. I. Karpov, Comput. Math. Applic. **58**, 965 (2009).